

Spectroscopy of PKS 0528-250: New Limits on CO Absorption and Emission¹

Jian Ge, Jill Bechtold, Constance Walker, John H. Black²
Steward Observatory, University of Arizona, Tucson, AZ 85721

Received _____; accepted _____

arXiv:astro-ph/9708104v1 12 Aug 1997

¹Observations here were obtained with the MMT, a joint facility of the university of Arizona and the Smithsonian Institution; and the NRAO 12 Meter Telescope. The NRAO is a facility of the National Science Foundation operated under cooperative agreement by Associated Universities, Inc.

²Current address: Onsala Space Observatory, Chalmers University of Technology, S-439 92 Onsala, Sweden

ABSTRACT

We have obtained a moderate resolution spectrum of the quasar PKS 0528-250 with the Red Channel Spectrograph on the Multiple Mirror Telescope (MMT) in order to study a damped Ly α absorption line system at $z = 2.8115$. We obtain a new upper limit for the CO column density for the $z = 2.8108$ velocity component in the $z = 2.8115$ damped Ly α system. The ionization of different species in this component rules out a quasar spectral energy distribution (SED) as the ionization field, and implies an ultraviolet radiation field intensity a few times that of the Milky Way value. The estimated total number density is $n(\text{H}) \sim 20 \text{ cm}^{-3}$. The physical size for the $z = 2.8108$ component implied by these models is about 40 parsecs. The ionization of different species also suggests a structure with a hot intercloud medium associated with a H I cloud in this component, that is, most low ionized ions are from the cold medium where photoionization and photodissociation dominates. The highly ionized species may be from the intercloud medium where collisional ionization dominates. We also present newly identified Ni II absorption lines in the $z = 2.1408$ and $z = 2.8115$ damped Ly α systems. The derived depletion of nickel by dust confirms previous results that the dust-to-gas ratio in these two damped Ly α systems is about 10% of the Milky Way ratio. Millimeter wavelength observations obtained at the NRAO 12 meter telescope provide new upper limits on CO (3-2) emission in the $z = 2.8115$ damped Ly α system.

Subject headings: ISM: abundances – ISM: molecules – quasars: absorption lines – quasars: individual (PKS 0528-250)

1. Introduction

Damped Ly α quasar absorption line systems may be the high redshift analogs of present-day galactic disks (Wolfe *et al.* 1986). They dominate the cosmological mass density of neutral gas in the Universe and hence trace the bulk of material available for star formation at high redshifts (Lanzetta 1993). If the physical conditions in the damped Ly α systems are similar to those in Galactic interstellar clouds, the damped Ly α systems should show absorption from low-ionization species like C I, trace elements like Ni, Zn and Cr and molecules like H₂ and CO. Most of these species have been detected in absorption in the damped Ly α systems (e.g. Foltz *et al.* 1988; Meyer *et al.* 1986, 1987, 1989; Pettini *et al.* 1994, 1996; Ge, Bechtold & Black 1997; Ge & Bechtold, 1997), with the notable exception of CO. Detection of molecules at high redshift would provide a strong diagnostic for the conditions in the clouds that harbor them.

To detect absorption lines from C I, Ni II, Zn II, Cr II and CO, high signal-to-noise ratio (S/N) spectra are required because the expected lines are very weak. PKS 0528-250 is one of the brightest quasars known, $m(1450\text{\AA})=17.73$ (Sargent *et al.* 1989), and so is a good object for detailed work. Toward PKS 0528-250, there are two damped Ly α systems at $z = 2.1408$ and $z = 2.8115$. The $z = 2.8115$ damped Ly α system has $N(\text{H I}) = 2.24 \times 10^{21} \text{ cm}^{-2}$ and is one of the highest column density damped Ly α systems known (Møller & Warren 1993).

The $z = 2.8115$ damped Ly α system is a good candidate to detect C I and CO. Foltz *et al.* (1988) have detected H₂ absorption associated with it. Lanzetta (1994, private communication) and Songaila & Cowie (1995) have further confirmed this detection. The redshift for the H₂ absorption is $z = 2.8118$ (Lanzetta 1994, private communication). The column density of molecular hydrogen, $N(\text{H}_2) = 2.6 \times 10^{16} \text{ cm}^{-2}$, a factor of 10 larger than the upper limits for other damped systems (Songaila & Cowie 1995; Levshakov *et al.* 1992 and references therein). The molecular fraction $f=2N(\text{H}_2)/[2N(\text{H}_2)+N(\text{H I})]=1.2 \times 10^{-5}$ is similar to the Milky Way diffuse clouds (Savage *et al.* 1977). Previous observations show that the H₂, CO and C I column densities are correlated with each other in the Milky Way diffuse clouds, e.g. $N(\text{H}_2)/N(\text{C I})$ is $\sim 10^2 - 10^6$ and $N(\text{C I})/N(\text{CO})$ is ~ 10 (e.g. Federman *et al.* 1980). Thus, we expect that the C I and CO column densities are high enough to be detectable.

Møller & Warren (1993) detected Ly α emission at $z = 2.8121$. The detected Ly α line luminosity of $1.1 \times 10^{42} h^{-2} \text{ ergs s}^{-1}$ corresponds to a star formation rate (SFR) of $1.0 h^{-2} M_{\odot} \text{ yr}^{-1}$, if there is no attenuation by dust (we adopt $q_0 = 0.5$, $H_0 = 100 h \text{ km s}^{-1} \text{ Mpc}^{-1}$). The minimum size of the absorber is about $18 h^{-1} \text{ kpc}$.

To study the nature of the $z = 2.8115$ damped Ly α system we have conducted two kinds of observations: (1) high signal-to-noise optical spectroscopy covering the strongest absorption bands of the CO A-X system (0-0, 1-0, 2-0, 3-0, 4-0, 5-0, 6-0), C I λ 1560 and some Ni II lines; and (2) millimeter observations of CO (J=3-2) emission at 90 GHz. The observations are described in section 2. Identifications of absorption lines are discussed in section 3. We discuss our results in section 4 and give a summary in the final section.

2. Observations

2.1. Optical Spectroscopy

The observations of PKS 0528-250 were obtained on February 14, 1994 with the Loral 800×1200 CCD attached to the Red Channel Spectrograph on the MMT (Schmidt *et al.* 1989). The 1200 l/mm grating was used in first order with 1" × 180" slit, which resulted in spectral resolution of 2.0 Å (FWHM), measured from the comparison lamp lines. The seeing was 0.5" (FWHM). We took three 40 minute exposures with wavelength coverage from 5200 Å to 6100 Å. The quasar was stepped by a few arcseconds along the slit between each exposure to smooth out any residual irregularities in the detector response which remained after flat-fielding. An exposure of a He-Ne-Ar-Cd-Hg lamp and a quartz lamp were done before and after each exposure of the object to provide an accurate wavelength reference, a measure of the instrumental resolution, and a flat-field correction. Bias frames were also obtained. The spectra were reduced in the standard way using IRAF. The summed spectrum weighted by the signal-to-noise from the three exposures is shown in Figure 1. The signal-to-noise ratio is about 50 in most of the wavelength coverage.

The continuum was fitted iteratively using a cubic spline routine. First the spectrum was divided into some moderately wide bins (40 pixels) and averaged in each bin. Then a cubic spline was fit to these averaged points. Points which deviated negatively by more than two standard deviations were flagged as possible significant lines and rejected for subsequent iterations of the fit. This process was repeated about six times until the fit did not change, i.e. until the number of flagged pixels above the fit was about equal to the number of pixels below the fit and the reduced chi-squared of all unflagged pixels was near unity (Bechtold 1994).

Significant lines were found by measuring the equivalent width in a bin equal to 2.46 times the number of pixels of the FWHM of the comparison lines, and its error (c.f. Young, Sargent & Boksenberg 1982). All such bins where the equivalent width was significant at greater than or equal to 3 σ were flagged. The final equivalent width of each absorption line was measured by specifying the wavelength interval for each feature by hand. The central wavelengths, equivalent widths and their errors are listed in Table 1. The central wavelength of each line in Table 1 is the centroid, weighted by the depth of each pixel in the line profile below the continuum (c.f. Bechtold 1994). The error for the central wavelength shown in this table is from the uncertainty in the measurement of the equivalent width. We neglected the uncertainty from the wavelength calibration because the error from the wavelength calibration is very small, typically less than 0.02 Å. All reported wavelengths are vacuum and have been corrected to the heliocentric frame.

2.2. Radio Observations

Our millimeter observations of the $z = 2.8108$ damped Ly α system toward PKS 0528-250 were made in January 1994 at the NRAO 12 Meter telescope. All of the observations were done with the dual polarization SIS 3 mm mixer receiver, which provided a system temperature of 260 K at 90 GHz. The central frequency was set to 90.74093 GHz corresponding to the heliocentric redshifted CO (J=3-2) emission frequency of the $z = 2.8108$ damped Ly α system. The telescope half-power beam width (HPBW), θ_B , was 68". The frequency calibration was checked with observations of Orion A. The pointing was checked with observations of Q 0607-157.

The spectra were obtained using absolute position switching between the source position and a reference position 3' away in azimuth. We used a 256 channel filter bank spectrometer with a spectral resolution of 2MHz. We obtained 498 minutes of integration on source in four nights; scans were six minutes in length. Each scan had the same three bad channels removed before the scans were summed. Two noisy scans were omitted from the final summation. Before taking the mean of a channel, we eliminated channels with more than a 10σ deviation from a robust median. At that point, a final 1σ deviation of each channel was calculated (Walker *et al.* 1996). The final spectrum is shown in Figure 2, where a single linear baseline has been fitted (by iteratively throwing out channels with intensities greater than 3.5σ) and then removed. In Figure 2, the 1σ error is represented as a dashed line. The results are discussed in section 4.4.

3. Notes on Individual Systems

Table 1 lists identifications of absorption lines in the optical spectrum of 0528-250. The redshifts of absorption lines are consistent with those identified by previous authors (Morton *et al.* 1980; Meyer & York 1987; Sargent *et al.* 1989). A few weak lines in Table 1 have not been identified and may be spurious. The $z = 2.671$ and $z = 2.673$ C IV absorption line systems are newly identified by us. We describe the different redshift systems separately in the following.

$z_{ab} = 0.9442$ — The redshift agreement is good between the two components of the Mg II doublet. The equivalent widths for these two lines are about half the values obtained by Sargent *et al.* (1989). The discrepancy may be caused by line blending in their data.

$z_{ab} = 2.1408$ — The equivalent width of Al II λ 1671 from this damped Ly α system is consistent with that measured by other authors (Morton *et al.* 1980; Sargent *et al.* 1989). We identify the absorption line at $\lambda = 5849.26 \text{ \AA}$ as Al III λ 1863. The other member of the doublet, Al III λ 1860 at $\lambda = 5825.29 \text{ \AA}$, is blended with the strong absorption line Si II λ 1526 from the $z_{ab} = 2.8115$ damped Ly α system. We have confirmed the identifications of two weak absorption lines of Ni II λ 1709, Ni II λ 1741 by Meyer *et al.* (1989) and we identify another weak Ni II transition, Ni II λ 1751. We discuss these further in section 4.2.

$z_{ab} = 2.5381$ — The equivalent widths of the C IV doublet are statistically consistent with those obtained by other authors (Morton *et al.* 1980; Sargent *et al.* 1989). We have not detected absorption from Si II λ 1526 in our spectrum.

$z_{ab} = 2.6259$ — This C IV absorption line system is tentatively identified here. There is a Ly α absorption line at $\lambda = 4406.57\text{\AA}$ with $W_{obs} = 3.60\text{\AA}$ corresponding to $z_{ab} = 2.6248$ (Morton *et al.* 1980). However, it is blended with the Si IV λ 1402 line of the $z_{ab} = 2.1408$ damped Ly α system. The absorption lines at 5614.02 and 5622.57 \AA could also be the absorption lines of Co II $\lambda\lambda$ 1472, 1475 from the $z = 2.8115$ damped Ly α system.

$z_{ab} = 2.6710, 2.6732$ — These two C IV absorption line systems are first identified here. The C IV 1550 absorption line from the $z = 2.6710$ system is blended with the C IV 1550 line from the $z = 2.6732$ system. The $z = 2.6732$ system has a moderate Ly α absorption line in the Ly α forest at $\lambda = 4465.42\text{\AA}$ with $W_{obs} = 4.84\text{\AA}$ corresponding to $z_{ab} = 2.6732$ (Morton *et al.* 1980).

$z_{ab} = 2.8115$ — The equivalent widths of the strong absorption lines Si IV λ 1393, 1402, Si II λ 1526, C IV λ 1548, 1550 are consistent with earlier measurements of Morton *et al.* (1980), Meyer & York (1987) and Sargent *et al.* (1989). We have confirmed that the $z_{ab} = 2.8115$ system consists of at least two components with $z_{ab} = 2.8108$ (A₁) and $z_{ab} = 2.8132$ (A₂) respectively (Morton *et al.* 1980), corresponding to a velocity separation of 45 km s⁻¹. We have detected three Ni II absorption lines from the $z_{ab} = 2.8115$ system at better than the 3 σ level. The absorption line at $\lambda = 5222.84\text{\AA}$ is identified as Ni II λ 1370.13 at $z = 2.8119$ instead of C IV λ 1548.20 at $z = 2.3733$ by Chen & Morton (1984) because no absorption line was detected for C IV λ 1550.77 at the same redshift, and the equivalent width should be at least 0.32 \AA if both members of the doublet are unsaturated, compared to our 5 σ upper limit of 0.26 \AA . The Ni II λ 1370 and Ni II λ 1454 lines exhibit the same two redshift components as the low ionized ions Si II, Fe II, OI and Al II lines. The absorption line of Ni II λ 1467, which is weaker than Ni II λ 1370, 1454, does not exhibit two velocity components probably due to limited S/N and resolution. The lines of the ionized species, C IV λ 1548, 1550 and Si IV λ 1393, 1402 are seen from the $z_{ab} = 2.8108$ system only (Morton *et al.* 1980; Meyer & York 1987).

There is an absorption line at the wavelength corresponding to C I λ 1560.31 from the $z = 2.8115$ damped Ly α system at about the 4 σ significance level. The rest frame equivalent width of this line is $38 \pm 10\text{ m\AA}$ which is lower than the 2 σ upper limit of 50 m \AA given by Meyer *et al.* (1987). If this is the C I absorption line, then the column density of C I is $2.2 \pm 0.6 \times 10^{13}\text{ cm}^{-2}$, assuming that the line is on the linear part of the curve-of-growth. However, much higher quality spectrum with the resolution of about 8 kms⁻¹ and S/N ≈ 50 from the KECK HIRES by Songaila *et al.* (1995, private communication) rules out this identification. Their spectrum does not show any absorption lines from C I λ 1277.24 and C I λ 1328.83 to the 3 σ upper limit of $N(\text{C I}) \leq 6 \pm 2 \times 10^{12}\text{ cm}^{-2}$, which is much smaller than that from our data. The 4 σ absorption feature in our MMT spectrum is probably a statistical artifact. Therefore, in what follows, we adopt the measurements by Songaila *et al.*

We have not detected absorption of the excited Si II* λ 1533 from the A₁ component in the $z = 2.8115$ damped Ly α system. The 3 σ upper limit of equivalent width is 0.118 \AA which will be used to derive the number density of hydrogen in this component (see section 4.1). The absorption of Si II* λ 1533 from the A₂ component in the $z = 2.8115$ damped system is blended with the Al

III λ 1863 line from the $z = 2.4108$ damped Ly α system.

The absorption line at $\lambda = 5519.40 \text{ \AA}$ is consistent with the CO A-X 1447.36 absorption line at $z_{ab} = 2.8132$. While CO λ 1447.36 is one of the strongest CO absorption lines (e.g. Field *et al.* 1983; Sheffer *et al.* 1992), we failed to detect the CO A-X $\lambda\lambda$ 1477.52, 1509.70 absorption lines which have similar strengths. The absorption line at 5519.40 \AA could also be the Co II λ 1448 line from the A₁ component of the $z = 2.8115$ damped system. Then the absorption line at 6000.53 \AA could be Co II λ 1574 lines from the same component. However, we also failed to detect Co II $\lambda\lambda$ 1466, 1480 in our spectrum which have similar strengths (Morton 1991). Therefore, the identification for the absorption at $\lambda = 5519.40 \text{ \AA}$ is uncertain.

4. Results and Discussion

4.1. Ionization

We have constructed models using the CLOUDY program (Ferland 1993) in order to investigate the ionization of the observed species, the spectrum of the UV ionizing radiation field, and the molecular fraction of the damped Ly α absorption line system at $z = 2.8115$.

The column densities for the species observed in the A₁ and A₂ components ($z = 2.8108$, $z = 2.8132$) of the $z = 2.81$ damped Ly α system are shown in Table 2. Because the resolution of the available spectra is insufficient to resolve the profiles of the lines listed in Table 2, we use a curve-of-growth analysis to infer column densities. We adopt the Doppler parameter $b = 60 \text{ km s}^{-1}$ for lines from the A₁ component and $b = 30 \text{ km s}^{-1}$ for lines from the A₂ component which are obtained from the curve-of-growth of Fe II (Meyer *et al.* 1989). If the absorption lines from the A₁ and A₂ components are blended with each other, we adopt $b = 100 \text{ km s}^{-1}$ obtained from fitting the Lyman lines (Foltz *et al.* 1988). However, the Si IV and C IV doublets in the A₁ component suggest that the Doppler parameter $b = 60 \text{ km s}^{-1}$ derived for Fe II lines does not apply. A higher Doppler parameter $b = 80 \text{ km s}^{-1}$ gives a better fit. Therefore, we adopt $b = 80 \text{ km s}^{-1}$ to calculate column densities of high ionization species, C IV, Si III, Si IV, N V, O VI in the A₁ component (Table 2). The b -values indicate there are probably several velocity components blended with each other in each line. However, the uncertainties in the column densities from single b -value curve-of-growth analysis may be less than a factor of 2 (Jenkins 1986). In fact, our derived column densities are consistent with the results given by Songaila & Cowie (1995), and Lu *et al.* (1996) based on higher resolution spectra.

As the input to CLOUDY, we adopt a metallicity of 10% of the solar value for all the elements in both A₁ and A₂ components of the $z = 2.8115$ damped Ly α system. We also consider the relative depletions by dust grains to Zn (about 0.6-0.7 in the logarithm unit) of heavily depleted elements such as Al, Si, Ca, Fe and Ni (Meyer *et al.* 1989). The dust-to-gas ratio is 10% of the

Milky Way and the constituents of dust grains are assumed the same as the Milky Way. The total neutral hydrogen column density $N(\text{H I})$ for the two components is $2.24 \times 10^{21} \text{ cm}^{-2}$ (Møller & Warren 1993). It is obtained by fitting the profile of the damped Ly α absorption line including the Ly α emission of the quasar because the redshift of the damped Ly α system ($z = 2.8115$) is about the same as that of the quasar ($z = 2.765$, Morton *et al.* 1980; Møller & Warren 1993). The neutral hydrogen column density for each of the two components in the $z = 2.8115$ damped Ly α system is uncertain. However, similar absorption of dominant ions of most species, such as O I, Si II, S II, Fe II, Ni II, in these two components suggest that the total neutral hydrogen column density in each component is also similar (cf. Table 2). We take the total column density as the approximate value for each of the components in the following discussion. There is therefore at least a factor of 2 uncertainty in the results from CLOUDY from the uncertainty in the neutral hydrogen column density in each velocity component.

Since the damped Ly α system is possibly near the quasar, the UV flux from the quasar can affect the ionization. We therefore have considered five types of spectral energy distributions (SED). Figure 3 shows these SEDs, along with the ionization potential of several ions.

4.1.1. Quasar SEDs

We use a power-law with index $\alpha = 1.0$ for $\lambda \geq 912\text{\AA}$, where $f_\nu \propto \nu^{-\alpha}$, measured for PKS 0528–250 by Sargent *et al.* (1989). We extrapolate the power to longer wavelengths which has little affect on our results. The quasar energy distribution at wavelengths shorter than the Lyman limit is uncertain. We therefore consider two different quasar SEDs: a(1) and a(2) (Figure 3). In these two models, the upper limit to the X-ray flux from the Einstein IPC at 1.0 keV is adopted for the wavelength longer than 0.2 keV (Wilkes *et al.* 1994). In a(1), we assume a power-law with index between the Lyman limit and 0.2 keV of $\alpha = 1.0$; this is the hardest spectrum that seems reasonable. In a(2), the SED between the Lyman limit and 0.2 keV is a power law connecting these two points.

4.1.2. 1 Gyr old constant SFR galaxy SED

We consider the models for the evolution of galactic SED’s, as calculated by Bruzual & Charlot (1993). The shape of the UV SED in the $\lambda \lesssim 3000\text{\AA}$ region does not change after about 0.1 Gyr if the SFR is constant, so we consider the SED of 1 Gyr old galaxy as representative. This is shown in the Figure 3 as model b. For an age less than 0.1 Gyr the SED is similar to the SED of an instantaneous starburst galaxy, which we consider in the next model.

4.1.3. 0.001 Gyr old instantaneous starburst galaxy SED

Compared with a 1 Gyr old constant SFR galaxy SED model, this model lacks hard UV photons because of the lack of AGB stars. This is shown in Figure 3 as model c.

4.1.4. Milky Way SED

We adopt the parameterization of the Milky Way radiation field by Black (1987). This includes starlight, cosmic background radiation, thermal emission of dust, hot interstellar gas heated by supernova remnants, stellar winds, and UV radiation from extragalactic sources such as QSOs and nearby active galaxies. The energy distribution between 13.6 eV and 54 eV is a power law extrapolated from other wavelengths. This is shown in Figure 3 as model d.

4.1.5. Power-law SED with spectral index $\alpha = 2.7$

The SED is a single power-law from radio to X-ray wavelengths. The energy distribution between the Lyman limit and 1100 Å is harder than the Milky Way SED, the constant SFR galaxy SED and the starburst galaxy SED, but is much softer than the quasar SEDs. This is shown in Figure 3 as model e.

Figure 4 shows the CLOUDY results for low ionization species. The ordinate is the column density of the various species, and the abscissa is the ionization parameter, $U = \phi(\text{H})/n(\text{H})c$, where $\phi(\text{H})$ is the surface flux of hydrogen-ionizing photons, $n(\text{H})$ is the total hydrogen number density (ionized, neutral, and molecular hydrogen), and c is the speed of light. CLOUDY shows that the column densities of O I, S II, Fe II, Si II and Ni II, which are the dominant ions of those species in the H I dominant regions, are not sensitive to different SED models over a large range of ionization parameter. Since all SED models give similar results for these ions, we only show the result from model e in Figure 4. The abundance of these ions from CLOUDY are consistent with the observed ones within about a factor of two indicating that we have a reasonable set of assumptions for the abundance and depletions.

Figure 5 shows the calculated and observed ratios of $N(\text{H}_2)/N(\text{C I})$ in the A_1 component of $z = 2.8115$ damped system. The common trend in the figure of $N(\text{H}_2)/N(\text{C I})$ vs. $N(\text{C I})$ can be explained by molecular hydrogen chemistry. The main destruction process of H_2 , photodissociation

through the process of spontaneous radiative dissociation by the Lyman and Werner bands, is initiated by discrete line absorptions. The lines are very narrow. Thus, the lines rapidly become optically thick, and then H₂ shields itself effectively, so that most of the hydrogen forms H₂ (e.g. van Dishoeck 1990). This is why we see a rapid increase of N(H₂)/N(C I) vs. N(C I) when the UV flux drops below a certain threshold. After that, the abundance of C I still increases as the UV decreases, but the abundance of H₂ increases slowly due to lack of formation material, hydrogen, which has already been changed into H₂. This is why the ratio of N(H₂)/N(C I) decreases after the rapid increase phase. The best fit to the observed ratios is the starburst model (b) and (c). Model (d) and (e) can fit the observed ratios within about 3σ. The quasar SED models (model a(1) and a(2)) cannot explain the observed ratios. The observed ratios are best explained by the soft UV energy distribution models, which suggest stars contribute most of the ionizing radiation field in the A₁ component of z = 2.8115 damped Lyα system. Thus, the SED model where the UV flux is mainly contributed by PKS 0528-250 can be ruled out, i.e. the distance between the A₁ component and the quasar is probably large enough (≳ 1 Mpc) that the UV flux from the quasar does not dominate the UV background radiation field in the A₁ component.

Figure 6 shows the CLOUDY results for the high ionization species assuming the total neutral hydrogen column density used in Figure 4. None of the model SEDs can explain the C IV, N V, Si IV, O VI and Si III column densities. Hence the absorption lines for these high ionization species are not coming from the same material as the absorption for the low ionization species. However, assuming the equilibrium between collisional ionization and radiative and dielectronic recombination, we find that T ∼ 1 × 10⁵ K can explain the relative ratios of these species (Shull & Van Steenberg 1982). The A₁ component may be a combination of a disk-like system and a halo, or warm and cold H I clouds associated with a hot intercloud medium.

Using the CLOUDY model, we can further estimate the average value of the UV radiation field along the sightline to the quasar in the A₁ component. In order to calculate this, we need to know the number density of neutral hydrogen. We estimate this density using the relative population ratio of the excited state Si II* λ 1533 Å to the ground state Si II λ 1526 Å. In the H I dominant region with density less than ∼ 10⁴ cm⁻³, this population ratio can be expressed as

$$\frac{N(Si II^*)}{N(Si II)} = \frac{n_e \langle \sigma v \rangle_e + n_p \langle \sigma v \rangle_p + n_H \langle \sigma v \rangle_H + n_{H_2} \langle \sigma v \rangle_{H_2}}{A_{10}}, \quad (1)$$

where n_e , n_p , n_H and n_{H_2} are, respectively, the electron, proton, hydrogen-atom and molecular hydrogen number densities, $\langle \sigma v \rangle$ is the collision rate, and A_{10} is the spontaneous transition probability (Bahcall & Wolf 1968). CLOUDY shows that the relative electron density n_e/n_H is about ∼ 10⁻² at the outside to ∼ 10⁻⁴ at the center of the cloud, and the equilibrium temperature is from ∼ 10³ K in the outside to ∼ 100 K in the center. We therefore can roughly neglect the contributions of the fine structure excitation by the proton and molecular hydrogen collisions (Bahcall & Wolf 1968). Then,

$$\frac{N(Si II^*)}{N(Si II)} \approx \frac{n_H \langle \sigma v \rangle_H + n_e \langle \sigma v \rangle_e}{A_{10}}, \quad (2)$$

where $\langle \sigma v \rangle_H = 1.3 \times 10^{-9} \exp(-413/T) \text{ cm}^3 \text{ s}^{-1}$ (Bahcall & Wolf 1968), and $\langle \sigma v \rangle_e = 3.8 \times 10^{-7} \exp(-413/T) \text{ cm}^3 \text{ s}^{-1}$ (Dufton & Kingston 1991). Taking the observed ratio $N(\text{Si II}^*)/N(\text{Si II}) < 1.41 \times 10^{-3}$, $T \sim 10^3 \text{ K}$ and $n_e/n_H \sim 10^{-2}$, we get $n_H < 47 \text{ cm}^{-3}$. CLOUDY gives a best fit $\log U \approx -2.9$ and -2.6 for the model b and c, respectively. Thus, the upper limit of the neutral hydrogen density implies an upper limit of $1\text{-}2 \times 10^9 \text{ cm}^{-2} \text{ s}^{-1}$ for the hydrogen-ionizing photon flux in the A_1 component. This upper limit is about 100 times larger than the Milky Way value of $\sim 1 \times 10^7 \text{ cm}^{-2} \text{ s}^{-1}$ (Black 1987). Because Si II* traces warm phase regions outside of the cloud (cf. Morton 1975), the above result is more suitable for outside region of the cloud. For the central part of the absorber cloud, the population ratio of the H_2 $J = 4$ to $J = 0$ levels, $N(J=4)/N(J=0) = 4.5 \times 10^{-3}$ (Songaila & Cowie, 1995), provides $Rn \approx 6 \times 10^{-17} \text{ s}^{-1}$, where R is the H_2 formation rate, $n = n(\text{H}) + 2n(\text{H}_2)$ (see Jura 1975 for details). We scaled the H_2 formation rate to $R \sim 3 \times 10^{-18} \text{ cm}^3 \text{ s}^{-1}$, assuming the dust-to-gas ratio is 10% that of the Milky Way. The density is then $\langle n \rangle \approx \langle n_H \rangle \sim 20 \text{ cm}^{-3}$. We therefore can use this value and other measurements to estimate the physical properties in the central part of the cloud and compare them with the CLOUDY results. In the central cloud where the kinetic temperature is around 100 K (Songaila & Cowie 1995), C II provides most of the electrons (e.g. Morton 1975), so

$$\frac{N(\text{CII})}{N(\text{HI})} \approx \frac{n(e)}{n(\text{H})} \approx 7.6 \times 10^{-5}, \quad (3)$$

where we have assumed a spatially homogeneous distribution of C II ions, electrons and hydrogen atoms. Thus, $n(e) \sim 10^{-3} \text{ cm}^{-3}$. The equation for C I photoionization equilibrium can be expressed as

$$n(e) = \frac{N(\text{CI})}{N(\text{CII})} \frac{\Gamma(I)}{\alpha(T)}, \quad (4)$$

where we have also assumed a homogeneous distribution of C I; the photoionization rate, $\Gamma(I)$ (s^{-1}), is a function of the radiation field intensity, I ; and $\alpha(T)$ ($\text{cm}^3 \text{ s}^{-1}$) is the radiative recombination rate coefficient, which is a function of kinetic temperature. The kinetic temperature in the H_2 containing cloud is between 74 K and 270 K, where 74 K is derived from the population ratio of the H_2 in the first excited rotational state to the ground rotational state and 270 K is derived from the $b = 1.5 \text{ km s}^{-1}$ for the H_2 absorption lines (Songaila & Cowie 1995). Therefore we choose $\alpha(T) = 1.0 \times 10^{-11} \text{ cm}^3 \text{ s}^{-1}$ (e.g. Snow 1977). From the measurements, we derive $N(\text{C I})/N(\text{C II}) \lesssim 3.5 \times 10^{-5}$. Putting these together, we get $\Gamma(I) \gtrsim 2.9 \times 10^{-10} \text{ s}^{-1}$ which is a factor of few larger than typical value of the $\Gamma(I) \sim 10^{-10} \text{ s}^{-1}$ in the Milky Way ISM (de Boer *et al.* 1973). This value is consistent with what we expect for the outer region of the cloud. Thus, all results derived here are consistent with those derived from the CLOUDY analysis.

We can further use these estimates of the physical parameters to estimate the size of the $z = 2.8108$ cloud. The averaged value for the electron density is derived to be $\langle n(e) \rangle \sim 10^{-3} \text{ cm}^{-3}$, $N(\text{C II}) \approx N(e) \sim \langle n(e) \rangle l$, thus, the physical size for the $z = 2.8108$ cloud, is $l \sim 40 \text{ pc}$.

For the A_2 component, the lack of highly ionized ions may mean that the A_2 component is not associated with any halo gas. The photoionization models described above cannot explain the lack

of H₂ and C I, along with the possible detection of CO, and special circumstances for molecule formation may apply.

In summary, we can account for the $z = 2.8108$ absorption line system (A₁) containing both hot and cold, neutral gas. The cloud medium contributes most absorption lines of low ionization species, while the hot medium contributes most absorption lines of highly ionized species. This structure is similar to that of the interstellar diffuse clouds in the Milky Way. The UV flux intensity in this absorber is a few times that of the typical value in the Milky Way ISM.

4.2. Dust Depletion of the Damped Ly α Systems

Pettini *et al.* (1994) have surveyed about a dozen damped Ly α systems to measure the abundance of Zn and Cr and have claimed that the metallicity of the damped Ly α systems at $z \sim 2$ is about 1/10 of the solar value. They used the relative abundance [Cr/Zn] to deduce the dust-to-gas ratio in the damped systems, which is about 1/10 of the Milky Way. This result is consistent with that from the dust reddening measurements of quasar spectrum slope by Pei *et al.* (1991). However, Lu *et al.* (1996) recently claimed that the overabundance of Zn relative to Cr may be intrinsic to the stellar nucleosynthesis in these absorbers instead of dust depletion (however, see Pettini *et al.* 1996; Smith *et al.* 1996). Here, we assume that the underabundance of Cr and Ni relative to Zn is caused by dust depletion. Compared with Cr, Ni is perhaps a better element to use to deduce depletion. Like Zn and Cr, Ni is an iron group element and it traces Fe to about [Fe/H] ~ -2.5 or even lower (Wheeler *et al.* 1989; Ryan *et al.* 1991). Ni is also more heavily depleted than Cr in the Milky Way (Jenkins, 1987): 0.35% Ni remains in the gas phase compared to 0.62% for Cr in the diffuse cloud toward ξ Per (Cardelli *et al.* 1991). Because the ionization potential of Ni I is 7.635 eV which is smaller than that of H I, but the ionization potential of Ni II is 18.168 eV which is larger than that of H I, Ni II is the dominant species of Ni in the neutral hydrogen dominant region. Consequently, the ratio of N(Ni II)/N(H I) can reflect that of Ni/H gas phase abundance without the need to account for unobserved ion stages. For example, under the condition that best fits the ionization structure of the A₁ component in the $z = 2.8115$ damped Ly α system, model (b), $\log U = -2.9$ and $n(\text{H})=1 \text{ cm}^{-3}$, $N(\text{Ni II})/N(\text{Ni}) = 97.7\%$. Moreover, there are more UV absorption lines of Ni II than Cr II. If we can observe more than two weak absorption lines of Ni II, we can use a curve-of-growth analysis to get a more accurate estimate of the column density. Another potential advantage of using Ni II instead of Cr II is that the Ni II transitions are observable with ground-base telescopes until redshifts about 5 without strong sky emission because the strong UV transitions of Ni have rest wavelengths between 1400 and 1700 Å compared to ~ 2000 Å for Cr and Zn.

Our measured equivalent widths of Ni II λ 1709, Ni II λ 1741 and Ni II λ 1751 in the $z_{ab} = 2.1408$ system correspond to column densities $3.4(\pm 1.1) \times 10^{13} \text{ cm}^{-2}$, $3.8(\pm 0.9) \times 10^{13} \text{ cm}^{-2}$ and $3.2(\pm 0.9) \times 10^{13} \text{ cm}^{-2}$, respectively, when we adopt a Doppler parameter $b = 30 \text{ km s}^{-1}$

(Meyer *et al.* 1989). They are consistent with the values obtained by Meyer *et al.* The average column density of Ni II is $3.5(\pm 0.5) \times 10^{13} \text{ cm}^{-2}$. The H I column density in this system is $5(\pm 1) \times 10^{20} \text{ cm}^{-2}$ (Morton *et al.* 1980). Thus, Ni/H is $7.0(\pm 0.2) \times 10^{-8}$, implying that Ni is depleted by no more than a factor of 27 ± 4 in the $z_{ab} = 2.1408$ damped Ly α system with respect to the solar ratio of 1.9×10^{-6} (Withbroe 1971) or $[\text{Ni}/\text{H}] = -1.43 \pm 0.06$. The upper limit of N(Zn II), $2.6 \times 10^{12} \text{ cm}^{-2}$, measured by Meyer *et al.* (1989) indicates that the metallicity in the 2.1408 system is $\leq 10\%$ of solar abundance. The measured residual depletion in the $z = 2.1408$ damped Ly α system is $[\text{Ni}/\text{Zn}] \geq -0.55$. For comparison, $[\text{Ni}/\text{Zn}] = -1.92$ in the diffuse cloud toward ξ Per of the Milky Way which has $N(\text{H}) = 1.97(\pm 0.35) \times 10^{21} \text{ cm}^{-2}$ (Cardelli *et al.* 1991). This is the typical value in the Milky Way (c.f. Jenkins 1987). The limit for $[\text{Ni}/\text{Zn}]$ implies that dust grains in the $z = 2.1408$ damped Ly α system contain about 70% of the total Ni, while dust in our Galaxy contain about 99% of the Ni. Thus, the dust-to-gas ratio is $\leq 7\%$ of that in the Milky Way. The low dust content implies an inefficient molecular hydrogen formation rate, which suggests low total molecular mass. Hence, if the measured dust-to-gas ratio is typical of the interstellar medium in the $z = 2.1408$ damped Ly α system, our result is consistent with nondetection of CO emission by Wiklind & Combes (1994), who obtained an upper limit for the total molecular mass of $3.2 \times 10^{11} h^{-2} M_{\odot}$ integrating over 1100 km s^{-1} , but not consistent with the huge amount of molecular mass, $M(\text{H}_2) = 7 \times 10^{11} h^{-2} M_{\odot}$, reported by Brown & Vanden Bout (1993).

The column densities for the newly identified Ni II λ 1370, Ni II λ 1454 and Ni II λ 1467 lines in the $z = 2.8115$ damped Ly α system are shown in Table 2. The average column density of Ni II is $6.5(\pm 0.6) \times 10^{13} \text{ cm}^{-2}$ in the A₁ component and $3.3(\pm 0.5) \times 10^{13} \text{ cm}^{-2}$ in the A₂ component. Together, we get $9.8(\pm 0.8) \times 10^{13} \text{ cm}^{-2}$ for the two components which is consistent with the column density obtained by Meyer *et al.* (1989) obtained by measuring the equivalent widths of Ni II λ 1709 and λ 1741. The H I column density for the 2 velocity components together in the damped system is $2.24(\pm 0.05) \times 10^{21} \text{ cm}^{-2}$ (Møller & Warren 1993). Thus, Ni/H is $4.4(\pm 0.2) \times 10^{-8}$, so that Ni is depleted by no more than a factor of 43 ± 2 with respect to the solar value or $[\text{Ni}/\text{H}] = -1.63 \pm 0.02$. The depletion of Zn is $[\text{Zn}/\text{H}] = -0.91$ (Meyer *et al.* 1989), so the metallicity is about 10% of the solar value. The residual depletion of Ni relative to Zn, $[\text{Ni}/\text{Zn}] = -0.72$ which means about 80% of the Ni is contained in dust grains. Consequently, the dust-to-gas ratio is about 8% of that of the Galaxy if dust grains cause the depletion of Ni relative to Zn.

4.3. CO absorption

In Figure 7, we show our spectra which cover the five ultraviolet CO bands (A-X 0-0, 1-0, 2-0, 3-0, 4-0). We mark the central positions of the CO lines of the two velocity components ($z = 2.8108, 2.8132$) in each spectrum. The CO 3-0 λ 1447 line exhibits absorption at 5887.47 \AA at the expected position of $z = 2.8132$ within the uncertainties. If this identification is correct, the CO column density is $4.7(\pm 1.6) \times 10^{13} \text{ cm}^{-2}$ assuming the line is unsaturated. However, the absorption line at 5887.47 \AA could also be the Co II 1448 line at $z = 2.8117$. The corresponding

column density is $3.9(\pm 1.3) \times 10^{13} \text{ cm}^{-2}$, which is consistent with the upper limit obtained by Songaila & Cowie (1995).

In order to improve the CO column density limit in the A_1 component, we constructed a composite CO spectra from the 5 CO lines using a method similar to that employed by Levshakov *et al.* (1989). To obtain the composite spectrum, we first shifted the spectral regions containing the CO absorption bands to rest frame 1477.52 \AA the wavelength of the CO A-X 2-0 band, which has the largest oscillator strength in the CO A-X system (Field *et al.* 1983), then normalized to the continuum, and averaged with each pixel weighted by the inverse of its variance. In order to avoid the possible effect of telluric absorption at $\lambda = 5892.08 \text{ \AA}$ and $z = 2.8108$ C IV absorption at 5900.16 \AA we used the fitted continuum value instead of the observed flux in our coaddition. The final composite spectrum is shown in Figure 7. No absorption of CO from the A_1 component is found. The 3σ upper limit to the equivalent width in the rest frame is 17 m\AA . Using the weighted mean of the oscillator strengths of the considered bands, we derive an upper limit on the CO column density of the A_1 component of $N(\text{CO}) < 2.9 \times 10^{13} \text{ cm}^{-2}$. Thus the ratio $N(\text{CO})/N(\text{H I}) \leq 1.3 \times 10^{-8}$ for the A_1 component, provided that the total neutral hydrogen absorption in the $z = 2.8115$ damped Ly α system is from this component.

4.4. CO emission

Figure 2 shows the summed spectrum of CO (J=3→2) from the damped Ly α system $z = 2.8115$ toward PKS 0528-250. We have not detected any emission from the $z = 2.8108$ and $z = 2.8132$ components. The 3σ upper limit of the observed integrated line intensity $I_{CO} = \int T_{mb} dv \leq 3\sigma_{rms} \Delta v / \sqrt{N_{chan}} = 0.141 \text{ K km s}^{-1}$ for the A_1 component, and $0.142 \text{ K km s}^{-1}$ for the $z = 2.8132$ component, where $\Delta v = 100 \text{ km s}^{-1}$ is the integrated velocity interval around the absorption components, and N_{chan} is the number of channels in the velocity interval of 100 km s^{-1} .

The CO luminosity for the $z = 2.8115$ damped Ly α system can be expressed,

$$L_{CO} = \Omega_S D_A^2 \int T_b dv, \quad (5)$$

where T_b is the brightness temperature of the source, Ω_S is the solid angle subtended by the source, and D_A is the angular size distance.

$$D_A = D_L / (1 + z)^2, \quad (6)$$

D_L is the luminosity distance,

$$D_L = c H_0^{-1} q_0^{-2} \{z q_0 + (q_0 - 1) [\sqrt{(2q_0 z + 1)} - 1]\}. \quad (7)$$

The observed temperature of the source T_{mb} is defined as

$$T_{mb} = \frac{\int_{\Omega_S} \int \frac{T_b(\theta, \phi)}{(1+z)} P(\theta, \phi) d\Omega}{\int_{4\pi} P(\theta, \phi) d\Omega}, \quad (8)$$

$P(\theta, \phi)$ is the normalized power pattern, and the factor $(1+z)$ is from the expansion of the universe. Moreover, the angular size of about $2.5''$ for the Ly α emission region in the $z = 2.8115$ damped Ly α system (Møller & Warren 1993) is much smaller than the beam size of the telescope of $68''$, so if the CO emission region has similar size as the Ly α emission region, then T_{mb} can be further expressed as

$$T_{mb} \approx \frac{T_b \Omega_S}{(1+z) \Omega_B}, \quad (9)$$

where $\Omega_B = \pi(\theta_B)^2/4 \ln 2$ is the telescope beam solid angle. Then the CO line luminosity can be expressed as

$$L_{CO} = I_{CO} \Omega_B D_L^2 (1+z)^{-3} K km s^{-1} pc^2, \quad (10)$$

The molecular mass can be written as

$$M_{H_2} = \alpha L_{CO}, \quad (11)$$

where α is the CO to H₂ conversion factor. Adopting the standard conversion factor, $\alpha = 4.8 M_\odot (K km s^{-1} pc^2)^{-1}$ (Sanders *et al.* 1991), we obtain a 3σ upper limit for the total molecular mass of $1.87 \times 10^{11} h^{-2} M_\odot$ in the A₁ component, and $1.88 \times 10^{11} h^{-2} M_\odot$ in the A₂ component. These upper limits are about a factor of two better than previous observations of Wiklind & Combes (1994) applying the same model assumptions to their T_b .

However, the adopted standard conversion factor could introduce some uncertainty in the total molecular mass derived here. It can be easily shown that the conversion factor α for gravitationally bound (virialized) clouds, $\alpha \propto \sqrt{n(H_2)}/T_b$. Hence, the total molecular mass in the $z = 2.8115$ damped Ly α system could be overestimated if the clouds in it have a higher brightness temperature than the Milky Way clouds, whereas the total mass could be underestimated if the clouds have higher density. Furthermore, there is a weak dependence of α on the CO abundance, $\alpha \propto [X(CO)]^{-1/4}$ (Radford *et al.* 1991). If the CO abundance in the $z = 2.8115$ damped Ly α system is considerably lower than the Milky Way molecular clouds, the abundance effect will lead to an underestimate of the total amount of the molecular gas. From these considerations, the uncertainty in estimating the molecular mass for the $z = 2.8115$ damped Ly α system is a factor of a few.

For comparison, the total molecular mass in the Milky Way is $2 \times 10^9 M_\odot$ (e.g. Sanders *et al.* 1991), the total molecular mass in the ultraluminous IR galaxy Arp 220 is $2 \times 10^{10} M_\odot$ (e.g. Solomon *et al.* 1990), and the total molecular mass of the hyperluminous IR galaxy F10214+4724 at $z = 2.286$, is $1.1 \times 10^{10} h^{-2} M_\odot$ (e.g. Downes *et al.* 1995). Thus, the derived upper limit of the molecular mass in the $z = 2.8115$ damped Ly α system is higher than any ultraluminous IR galaxy.

On the other hand, our optical observations suggest that this damped Ly α system is an analog of a Milky Way-like normal galaxy at high redshift. In order to detect the molecular mass in this system if it is similar to the Milky Way, an rms/channel of $\sim 10^{-2}$ mK is needed, using the same telescope size, system temperature and bandpass. This requires an integration time 10,000 times longer than obtained here. However, interferometers could be used to reach interesting detection levels (e.g. Omont *et al.* 1996; Ohta *et al.* 1996).

5. Summary

Our main results are the following.

1. The ionization of different species in the A₁ component of the $z = 2.8115$ damped Ly α system rules out the possibility that the quasar UV flux dominates the UV ionizing field in this component, i.e. the quasar should be more than ~ 1 Mpc away from the damped Ly α system. The ionization further suggests that the shape of the UV background radiation field in this component is similar to the Milky Way. The UV field intensity is a few times that of the Milky Way value which further implies that the SFR in this component is probably similar to the SFR of the Milky Way if the total mass in this component is similar to the Milky Way. This result is consistent with the results from Ly α observations (Møller & Warren 1993). The physical size for this component is about 40 pc. The ionization of different species suggests a structure with a hot intercloud medium associated with a H I cloud in this component, i.e. most lowly ionized ions are from the cold medium where photoionization and photodissociation dominates. Most highly ionized ions are from the intercloud medium where collisional ionization dominates.

2. We have not detected CO absorption in the rest UV spectrum from the A₁ component of the $z = 2.8115$ damped system. The 3σ upper limit of CO column density is $N(\text{CO}) \leq 2.9 \times 10^{13} \text{ cm}^{-2}$ for this component. The ratios of the $N(\text{CO})/N(\text{H I})$ and $N(\text{CO})/N(\text{H}_2)$ are in the range of the values for the Milky Way diffuse clouds (Federman *et al.* 1980). The absorption line at 5519.40 Å could be a CO absorption line from the A₂ component; however, it also could be a Co II absorption line from A₁ component. Higher resolution and higher signal-to-noise observations are needed to confirm the identification of this line.

3. Analysis of photoionization and photodissociation of H₂ and C I suggests that the ratio $N(\text{H}_2)/N(\text{C I})$ is a good indicator of the shape of the radiation field in the ISM of damped Ly α absorbers.

4. Newly identified Ni II absorption lines show that the dust-to-gas ratios in the $z = 2.1408$ and $z = 2.8115$ damped Ly α systems are about 10% of that of the Milky Way, which are consistent with previous results.

5. We have not detected CO (3-2) mm emission from the $z = 2.8115$ damped Ly α system. The 3σ upper limits for the mass of H₂ in the A₁ and A₂ components in the $z = 2.8115$ damped system

are $1.87 \times 10^{11} h^{-2} M_{\odot}$ and $1.88 \times 10^{11} h^{-2} M_{\odot}$, respectively. The results still cannot rule out the possibility that the $z = 2.8115$ damped Ly α system is similar in molecular mass to ultraluminous IR galaxies.

We are grateful to Dr. A. Songaila Cowie for providing important comments and data in advance of publication. We thank Dr. J. Shields for helpful discussions. We thank Dr. G. Ferland for providing his CLOUDY program. We thank Dr. G. Bruzual and Dr. S. Charlot for providing their Galaxy Isochrone Synthesis Spectral Evolution Library (GISSEL). We also wish to thank the staffs of MMT0 and NRAO for all of their help. This research was supported by NSF AST-9058510 and NASA grant NAGW-2201.

REFERENCES

- Bahcall, J. N. & Wolf, R. A. 1968, *ApJ*, 152, 701
- Bechtold, J. 1994, *ApJS*, 91, 1
- Bergeson, S.D., & Lawler, J.E. 1993, *ApJ*, 414, L137
- Black, J. H. 1987, in *Interstellar Processes* (Reidel Publishing Company), eds. Hollenbach, D. J. & Thronson, Jr. H. A. 731
- Brown, R. L & Vanden Bout, P. A. 1993, *ApJ*, 412, L12
- Bruzual, G. A. & Charlot, S. 1993, *ApJ*, 405, 538
- Cardelli J. A., Savage, B. D, Bruhweiler, F. C., Smith, A. M., Ebbets, D. C., Sembach, K. R., & Sofia, U. J. 1991, *ApJ*, 337, L57
- Chen, J. & Morton, D. C. 1984, *MNRAS*, 208, 167
- de Boer, K. S., Koppelaar, K., & Pottasch, S. R., 1973, *A&A*, 28, 145
- Downes, D., Solomon, P. M., & Radford, S. J. E., 1995, *ApJ*, 453, L65
- Dufton, P. L. & Kingston, A. E. 1991, *MNRAS*, 248, 827
- Federman, S. R., Glassgold, A. E., Jenkins, E. B. & Shaya, E. J. 1980, *ApJ*. 242, 545
- Ferland, G. J. 1993, Univ. of Kentucky, Department of Physics and Astronomy Internal Report.
- Field, R. W., Benoist d’Azy, O., Lavollee, M., Lopez-Delgado, R. & Tramer, A. 1983, *J. Chem. Phys.* 78, 2838
- Foltz, D. B., Chaffee, F. H. & Black, J. H. 1988, *ApJ*, 324, 267
- Ge, J., Bechtold, J., & Black, J.H. 1997, *ApJ*, 474, 67
- Ge, J., & Bechtold, J. 1997, *ApJ*, 477, L73
- Jenkins, E. B. 1986, *ApJ*, 304, 739
- Jenkins, E. B. 1987, in *Interstellar Processes* (Reidel Publishing Company), eds. Hollenbach, D. J. & Thronson, Jr. H. A. 533
- Lanzetta, K. M. 1993, in *The Environment and Evolution of Galaxies* (Kluwer Academic Publishers), ed. Shull, J. M. & Thronson, Jr. H. A. 237
- Levshakov, S. A., Foltz, C. B., Chaffee, F. H. & Black, J. H. 1989, *AJ*, 98, 2052
- Levshakov, S. A., Chaffee, F. H., Foltz, C. B. & Black, J. H. 1992, *A&A*, 262, 385
- Lu, L., Sargent, W.L.W., & Barlow, T.A., 1996, *ApJS*, in press
- Meyer, D. M., Black, J. H., Chaffee, F. H., Foltz, C. B. & York, D. G. 1986, *ApJ*, 308, L37
- Meyer, D. M. & York, D. G. 1987, *ApJ*, 319, L45
- Meyer, D. M., Welty, D. E. & York, D. G. 1989, *ApJ*, 343, L37

- Møller, P. & Warren, S. J. 1993, *A&A*, 270, 43
- Morton, D. C., 1975, *ApJ*, 197, 85
- Morton, D. C., Chen, J., Wright, A. E., Peterson, B. A., Jauncey, D. L. 1980, *MNRAS*, 193, 399
- Morton, D. C., York, D. G. & Jenkins, E. B. 1988, *ApJS*, 68, 449
- Morton, D. C., 1991, *ApJS*, 77, 119
- Ohta, K., Yamada, T. Kohno, K., Akiyama, M., & Kawabe, R. 1996, *Nature*, 382, 426
- Pei, Y.C., Fall, S.M., & Bechtold, J. 1991, *ApJ*, 378, 6
- Pettini, M., Smith, L. J., Hunstead, R. W. & King, D. L. 1994, *ApJ*, 426, 79
- Pettini, M., King, D.L., Smith, L.J., & Hunstead, R., 1996, Preprint
- Radford, S. J. E., Solomon, P. M. & Downes, D. 1991, *ApJ*, 368, L15
- Ryan, S. G., Norris, J. E. & Bessell, M. S. 1991, *AJ*, 102, 303
- Sanders, D. B. Scoville, N. Z. & Soifer, B. T. 1991, *ApJ*, 370, 158
- Sargent, W. L. W., Steidel, C. C. & Boksenberg, A. *ApJS*, 1989, 69, 703
- Savage, B. D, Bohlin, R. C., Drake, J. F. & Budich, W. 1977, *ApJ*, 216, 291
- Schmidt, G. D., Weymann, R. J. & Foltz, C. B. 1989, *PASP*, 101, 713
- Sheffer, Y., Federman, S. R., Lambert, D. L. & Cardelli, J. A. 1992, *ApJ*, 397, 482
- Shull, J. M. & Van Steenberg, M. 1982, *ApJS*, 48, 95
- Smith, L.J., Pettini, M., King, D.L., & Hunstead, R.W., 1996, Preprint
- Snow, T. P., 1977, *ApJ*, 216, 724
- Solomon, P. M. Radford, S. J. E.& Downes, D. 1990, *Ap J*, 348, L53
- Songaila, A. & Cowie, L. L. 1995, *AJ* submitted
- van Dishoeck, E. F. 1990, in *Molecular Astrophysics* (Cambridge University Press), ed. Hartquist, T. W. 55
- Walker, C. E. *et al.* 1996, in preparation
- Wheeler, J. C, Sneden, C. & Truran, Jr., J. W. 1989, *ARA&A*, 27, 279
- Wiklind, T. & Combes, F. 1994, *A&A*, 288, 41
- Wilkes, B. *et al.* 1994, *ApJS*, 92, 53
- Withbroe, G. L. 1971, in *The Mengal Symposium* (NBS Spec. Pub. 353), ed. Gebbie, K. B. (Washington: GPO), 127
- Wolfe, A. M., Turnshek, D. A., Smith, H. E., & Cohen, R. D. 1986, *ApJS*, 61, 249
- Young, P. J., Sargent, W. L. W., & Boksenberg, A. 1982, *ApJ*, 252, 10

Figure Captions

Figure 1.—The spectrum of PKS 0528-250 obtained with the MMT Red Channel Spectrograph. The lower curve presents the 1σ error as derived from count statistics in the object and night sky spectra. The features identified at better 3σ significance in Table 1 are indicated by tick marks.

Figure 2.—The summed CO(3→2) millimeter wavelength spectrum of PKS 0528-250 observed with NRAO 12 Meter telescope. The intensity scale is main-beam brightness temperature (K) and the velocity scale is the offset (km s^{-1}) from the optical redshift, $z = 2.81086$. The two velocity components are marked. A fit to the baseline has been subtracted. The upper line presents the 1σ error derived from all scans after removing bad scans.

Figure 3.—Spectral energy distributions adopted for photoionization calculations. a(1) and a(2) are quasar SEDs. (b). 1 Gyr old constant SFR galaxy SED. (c). 0.001 Gyr old instantaneous starburst galaxy SED. (d). Milky Way SED. (e). power-law SED with $\alpha = 2.7$. Ionization potentials for several ions are marked.

Figure 4.—Ionization models for the H I dominant region with $N(\text{H I}) = 2.24 \times 10^{21} \text{ cm}^{-2}$. The ordinate is the column density of various ions, the abscissa is the log of the ionization parameter U . The figure shows results of dominant ions, O I, Fe II, Si II, S II and Ni II in the model e—power-law SED model with $\alpha = 2.7$. Solid lines are from CLOUDY and dotted lines are the observed values.

Figure 5.— The relative ratios of $N(\text{H}_2)/N(\text{C I})$ vs. $N(\text{C I})$. The results are shown for SED models described in Figure 3. The vertical lines show the upper limit (3σ) of $N(\text{C I})$. The horizontal lines show the lower limit (3σ) of the ratio of $N(\text{H}_2)/N(\text{C I})$.

Figure 6.— Model predictions for the highly ionized species, O VI, N V, C IV, Si IV, Si III for the different SED models described in Figure 3. Solid lines are results from CLOUDY. Dotted lines are the observed values. The CLOUDY predictions for O VI and N V are out of the range for the SED model (c). O VI is out of the range for the SED model (b).

Figure 7.—Spectral regions including the CO A-X 0-0, 1-0, 2-0, 3-0, 4-0 absorption bands from the $z = 2.8108$ and 2.8132 components in the rest frame of the $z = 2.8108$ absorber toward PKS 0528-250. The positions of the absorption bands are indicated by tick marks. The lowest right panel is a composite spectrum obtained by combining the 2-0 band with the 0-0, 1-0, 3-0, 4-0 bands which are shifted to the wavelength of the 2-0 band.

Table 1. The identifications of absorption lines of QSO 0528-250

No.	$\lambda_{obs}(\text{\AA})$	$\sigma(\lambda)$	W_{obs}	$\sigma(W)$	SL	ID	z_{abs}
1	5221.93	0.12	0.392	0.040	9.9	NiII 1370	2.8113
2	5224.56	0.22	0.235	0.036	6.6	NiII 1370	2.8132
3	5247.71	0.07	1.875	0.049	37.9	AlII 1671	2.1409
(4)	5273.53	0.31	0.091	0.030	3.1	?	
(5)	5293.72	0.44	0.11	0.04	3.1	CaI 2722	0.9444
6	5312.28	0.06	3.792	0.054	70.6	SiIV 1393	2.8115
7	5346.69	0.09	2.850	0.057	50.2	SiIV 1402	2.8115
(8)	5370.41	0.41	0.128	0.038	3.4	NiII 1709	2.1413
9	5436.42	0.19	0.688	0.049	14.0	MgII 2796	0.9441
10	5450.20	0.11	0.476	0.036	13.1	MgII 2803	0.9440
11	5470.03	0.44	0.223	0.046	4.8	NiII 1741	2.1409
12	5477.68	0.09	0.892	0.041	21.7	CIV 1548	2.5381
13	5486.93	0.16	0.516	0.042	12.3	CIV 1550	2.5382
(14)	5502.70	0.35	0.107	0.033	3.2	NiII 1751	2.1410
(15)	5519.40	0.63	0.123	0.039	3.1	CO 1447(?)	2.8136
						Co II 1448(?)	2.8117
16	5545.07	0.27	0.247	0.039	6.3	NiII 1454	2.8114
17	5595.11	0.53	0.145	0.041	3.5	NiII 1467	2.8120
18	5607.70	0.26	0.102	0.029	3.5	Si II1526	2.6731
19	5614.02	0.42	0.153	0.038	4.1	CIV 1548(?)	2.6262
(20)	5622.57	0.34	0.107	0.032	3.4	CIV 1550(?)	2.6256
21	5678.62	0.13	0.391	0.035	11.1	Si II 1808	2.1408
22	5683.49	0.14	0.201	0.030	6.6	C IV	2.6710
23	5687.23	0.15	0.665	0.047	14.3	CIV 1548	2.6734
24	5695.89	0.18	0.360	0.040	9.1	CIV 1550	2.6729
25	5818.72	0.02	5.008	0.034	147.4	SiII 1526	2.8113
	5823.09	0.03	3.274	0.033	98.4	SiII 1526, AlIII 1855	2.8142
26	5849.26	0.18	0.385	0.038	10.2	AlIII 1863	2.1401
27	5857.48	0.28	0.121	0.030	4.0	?	
(28)	5887.47	0.21	0.079	0.025	3.1	CO 1544 (?)	2.8122
29	5892.08	0.14	0.32	0.04	8.1	telluric line	
30	5900.16	0.04	4.889	0.051	95.5	CIV 1548	2.8110
31	5909.85	0.04	3.721	0.049	76.5	CIV 1550	2.8110
32	5947.05	0.29	0.145	0.037	3.9	(?)	
33	6000.53	0.32	0.144	0.039	3.7	Co 1574(?)	2.8110

Table 2. Line Strengths and Column Densities ^a

Species	λ	f^d	z=2.8108		z=2.8132		
			$W_\lambda(\text{\AA})$	$N(\text{cm}^{-2})_{b=60\text{km s}^{-1}}$	$N(\text{cm}^{-2})_{b=80\text{km s}^{-1}}$	$W_\lambda(\text{\AA})$	$N(\text{cm}^{-2})_{b=30\text{km s}^{-1}}$
Al II (A ₁ +A ₂) ^b	1670.788	1.88	2.100	4.4×10^{14}		2.100	4.4×10^{14}
C I	1560.310	0.0822		$\leq 6.0 \times 10^{12e}$		<0.032	$<1.8 \times 10^{13}$
C II (A ₁ +A ₂ +A ₂ [*]) ^b	1334.532	0.118	2.29	1.7×10^{17}		2.29	1.7×10^{17}
C II*	1335.702	0.118				0.312	3.6×10^{14}
C III (A ₁ +A ₂) ^b	977.020	0.768	1.89	7.6×10^{16}		1.89	7.6×10^{16}
C IV	1548.202	0.194	1.28	5.6×10^{15}	1.3×10^{15}		
C IV	1550.774	0.0970	0.976	2.0×10^{15}	1.1×10^{15}		
Si I ^c	1845.520	0.229	<0.105	$<1.6 \times 10^{13}$		< 0.105	$<1.6 \times 10^{13}$
Si II	1808.013	0.00208	0.397	8.5×10^{15}		0.094	1.7×10^{15}
Si II* ^c	1533.431	0.13	<0.031	$<1.2 \times 10^{13}$			
Si III	1206.500	1.66	1.14	1.9×10^{15}	3.6×10^{14}		
Si IV	1393.755	0.528	0.995	7.9×10^{14}	3.0×10^{14}		
Si IV	1402.770	0.262	0.748	4.6×10^{14}	3.0×10^{14}		
S I ^c	1425.030	0.181	<0.031	$<9.5 \times 10^{12}$		<0.031	$<9.5 \times 10^{12}$
S II	1250.583	0.00535	0.157	2.7×10^{15}		0.131	2.6×10^{15}
	1253.808	0.0107	0.315	...		0.236	...
S III (A ₁ +A ₂) ^b	1012.504	0.0355	0.622	3.2×10^{15}		0.622	3.2×10^{15}
O I	1302.169	0.0486	1.36	2.1×10^{17}		0.70	1.1×10^{17}
O VI	1031.927	0.13	0.97	4.0×10^{16}	5.2×10^{15}		
N V	1238.821	0.157	0.247	1.5×10^{14}	1.4×10^{14}		
Fe II	2249.879	0.0018	0.160	1.8×10^{15}		0.046	3.6×10^{14}
	2260.781	0.0028	0.260	...		0.046	...
	2374.461	0.0395	1.201	...		0.342	...
Ni II	1741.549	0.068	0.116	6.9×10^{13}		0.072	3.8×10^{13}
	1709.600	0.047	0.101	...		0.056	...
	1370.132	0.100	0.103	...		0.062	...
	1454.842	0.0515	0.065	...		0.027	...
Ni II (A ₁ +A ₂) ^b	1467.756	0.0149	0.038	1.3×10^{14}		0.038	1.3×10^{14}
Co II (?)	1448.011	0.04516	0.032	3.9×10^{13}			
CO A-X (?)	1447.359	0.0360				0.032	6.4×10^{13}
CO (composite) ^c			<0.017	$< 6.1 \times 10^{12}$			
H ₂				2.6×10^{16}			

^a Rest frame equivalent widths, obtained from Morton et al. (1980), Chen & Morton (1984), Foltz et al. (1988), Meyer et al. (1989), Songaila & Cowie (1995) and our observations.

^b We adopt $b = 100 \text{ km s}^{-1}$ when the absorption lines from the $z = 2.8108$ (A₁) and the $z = 2.8132$ (A₂) components are blended.

^c The upper limits are calculated for 3σ deviations.

^d Oscillator strengths, f , are from Morton (1991) except that for Si II λ 1808 is from Bergeson & Lawler (1993) and Si II* 1533 is from Hibbert et al. (1992).

^e Songaila (1995, private communication).

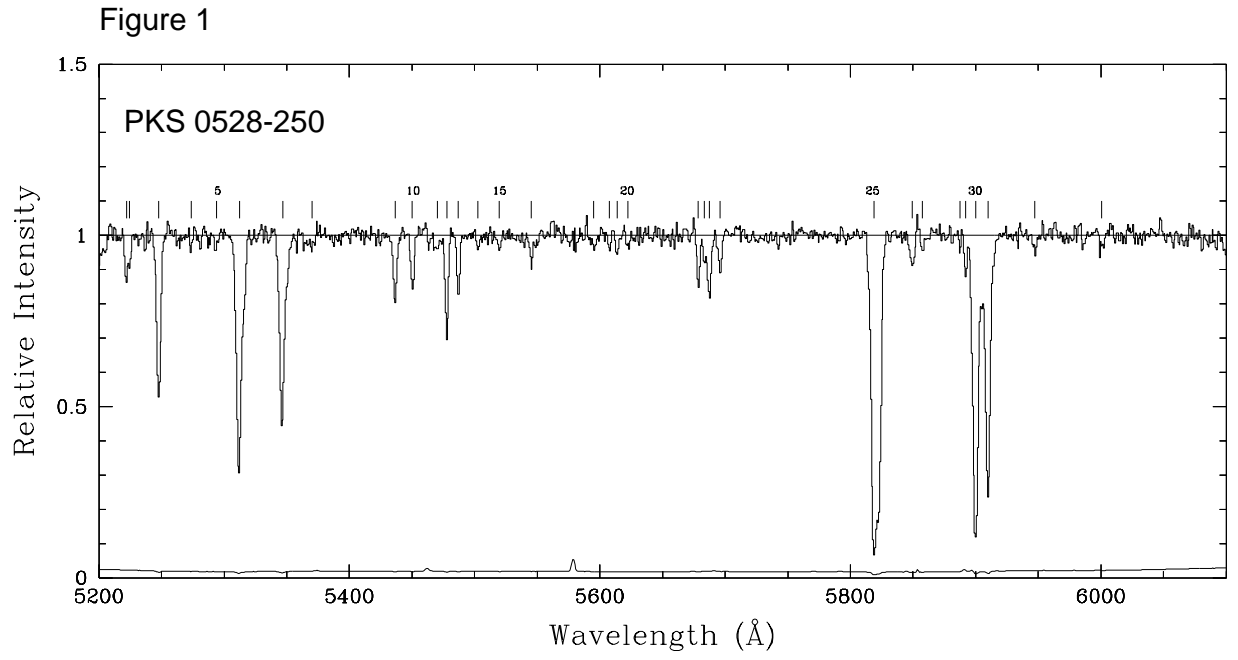


Figure 2

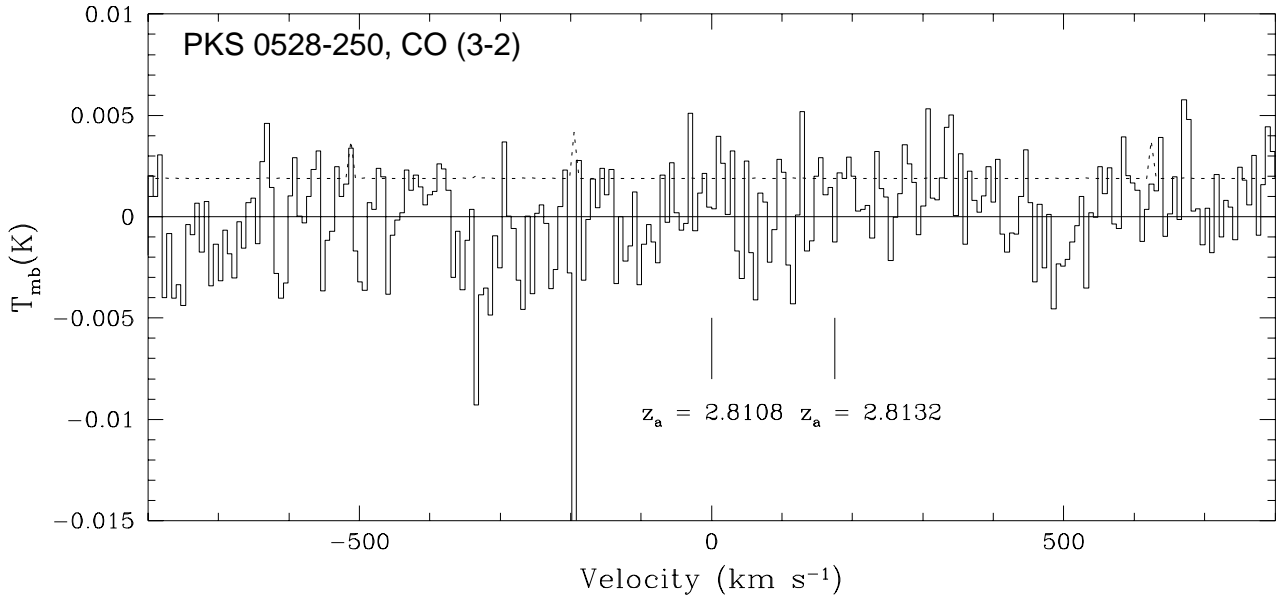


Figure 3

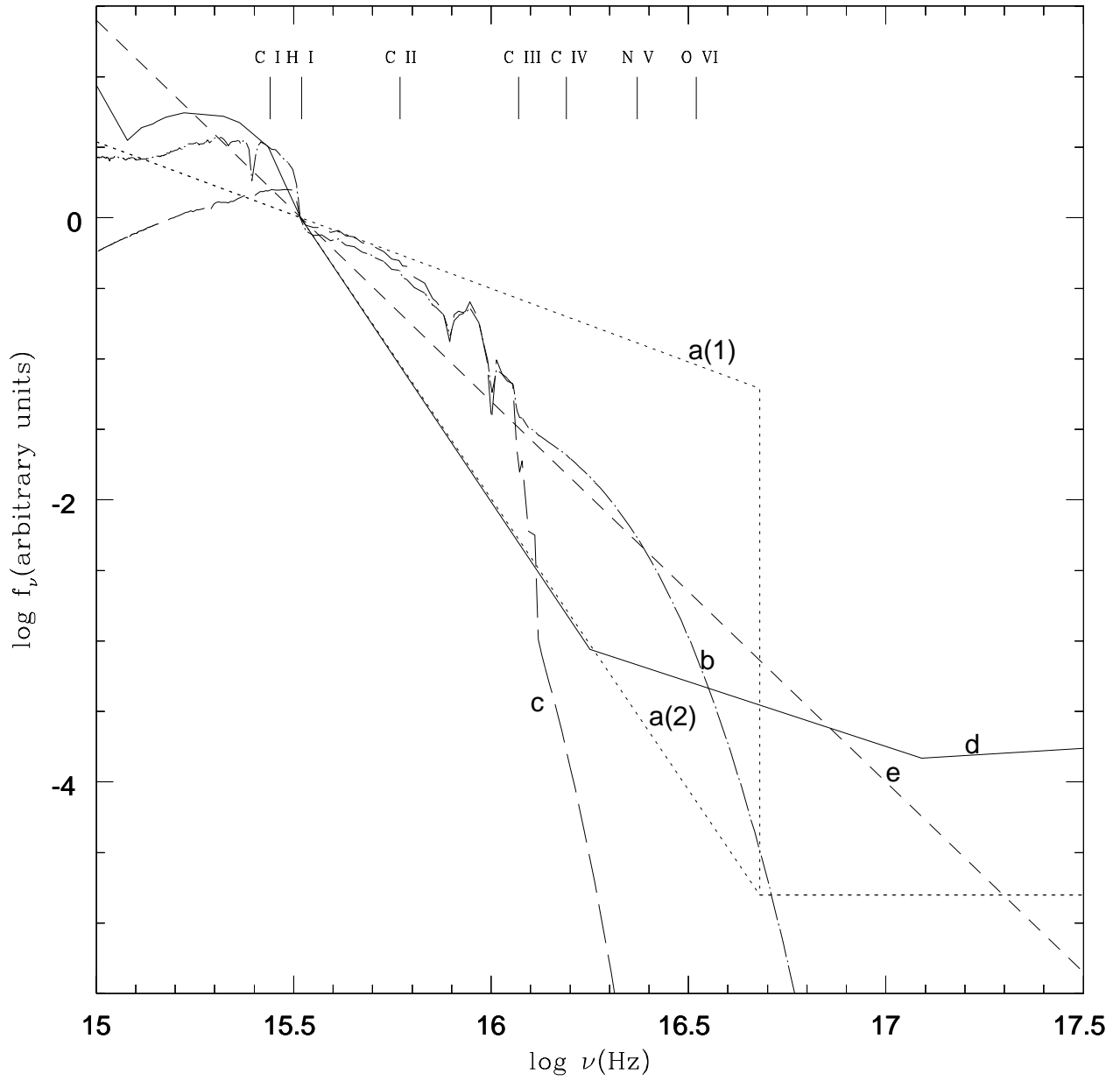


Figure 4

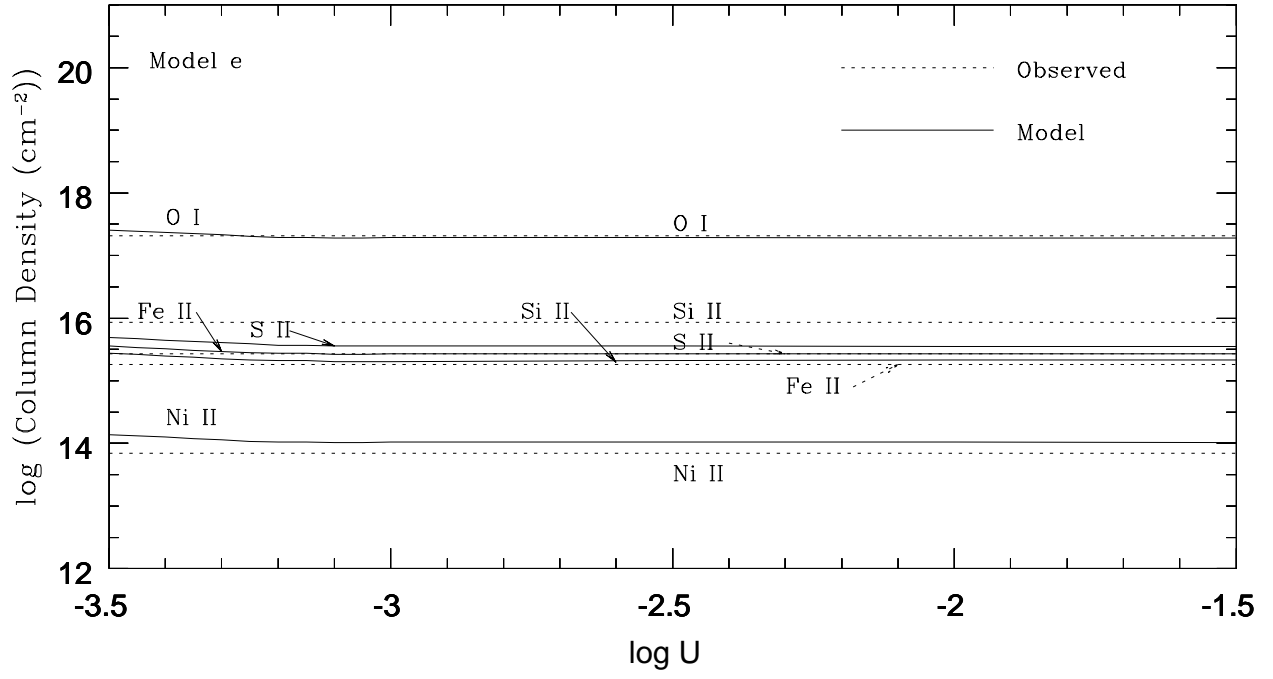


Figure 5

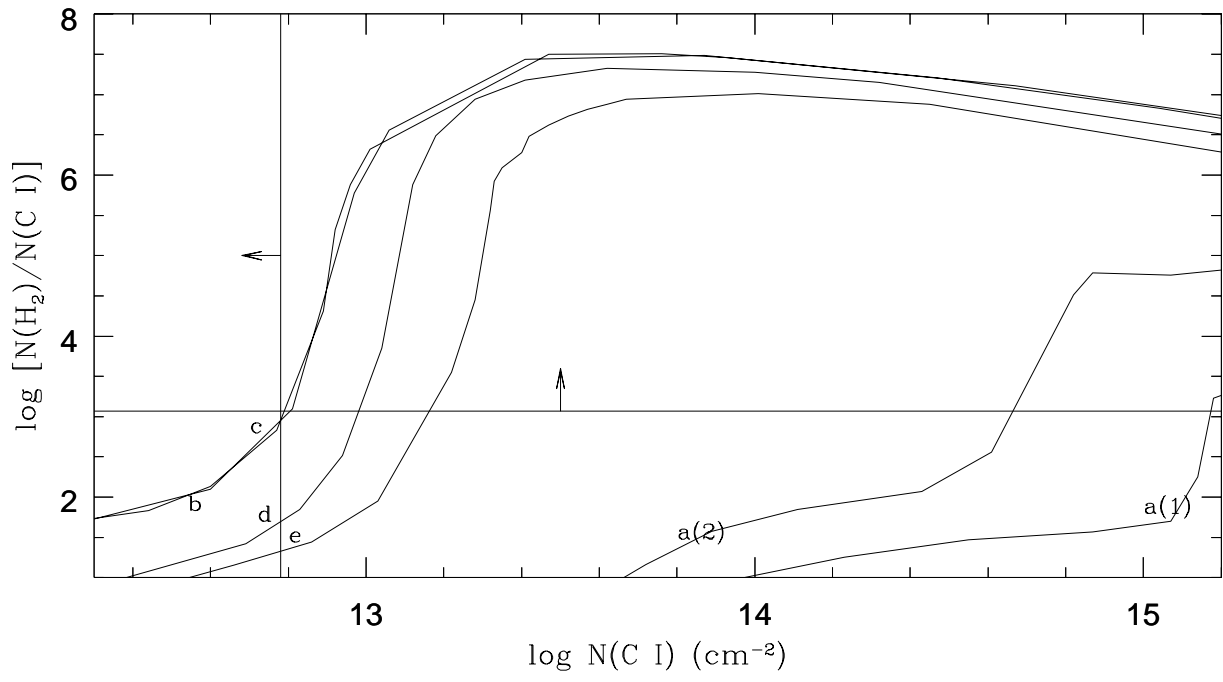


Figure 6

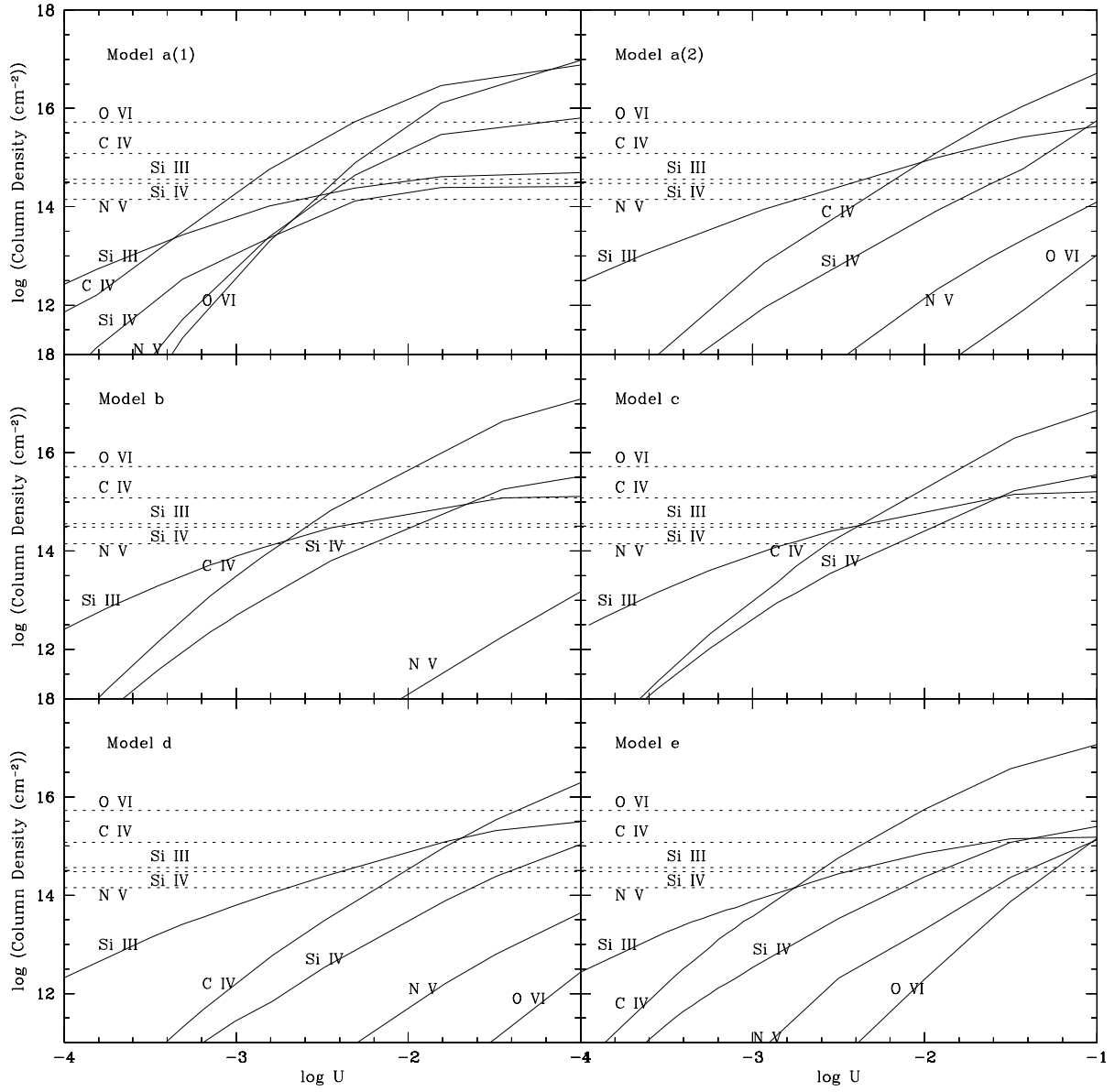


Figure 7

